The origins of IgA-secreting cells in the acinar structures of the nasal turbinates

Jingjing Liu[1], Liat Stoler-Barak[1], Hadas Hezroni-Bravyi[1], Adi Biram[1], Sacha Lebon[2], Natalia Davidzohn[2], Merav Kedmi[3,4], Muriel Chemla[3,4], David Pilzer[3,4], Marina Cohen[5], Ori Brenner[5], Moshe Biton[2] and Ziv Shulman[1,6,*]

Extended information

Extended Data Figure 1

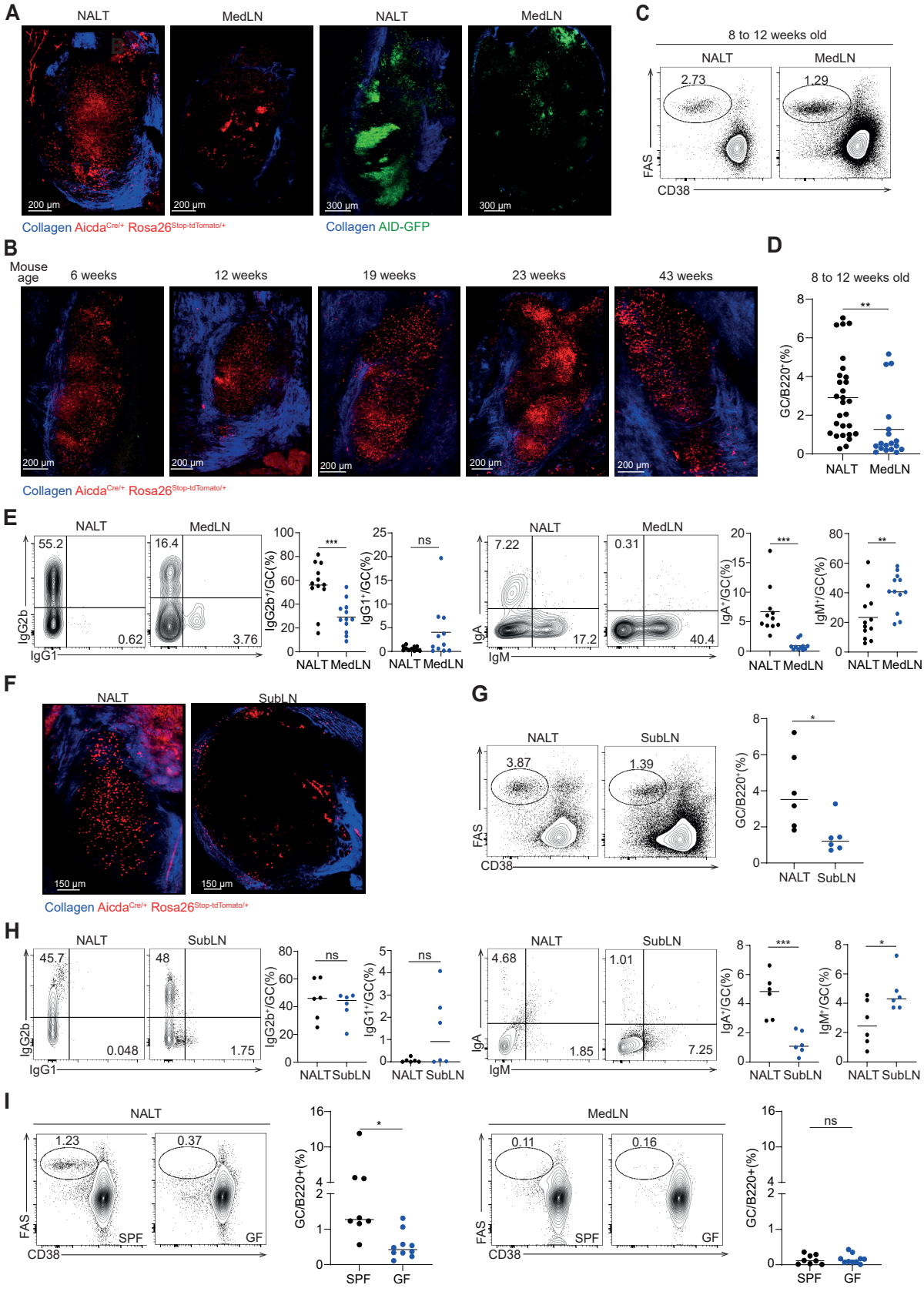

Extended Data Fig. 1: NALT hosts commensal-driven chronic germinal centers.

(A B) Representative TPLSM images of NALT and MedLN. (A) LNs derived from naïve $Aicda^{Cre/+}$ $Rosa26^{Stop\text{-}tdTomato/+}$ mice (left) or AID-GFP^{+} (right) mice. Scale bars, 200µm, 300 µm. n= 4-5, 7 independent experiments. (B) NALT derived from 6 weeks to 43 weeks old $Aicda^{Cre/+}$ $Rosa26^{Stop\text{-}tdTomato/+}$ mice. Scale bars, 200µm. n=1-3, 3 independent experiments. (C D) Representative plots and quantification of GC B cells from NALT and MedLN. LNs derived from naïve C57BL/6 SPF mice. $B220^{+}$ population gated from the $CD45^{+}$ compartment; FAS^{+} $CD38^{-}$ GC population gated from the $B220^{+}$ compartment. For NALT, n=28, mean of GC (%)=2.908, SEM=0.3893; for MedLN, n=18, mean of GC (%)=1.27, SEM=0.4006; data pool from 9 independent experiments. (E) NALT and MedLN cells derived from naïve C57BL/6 SPF mice. IgA^{+}, $IgG1^{+}$, $IgG2ab^{+}$ and IgM^{+} population gated from FAS^{+} $CD38^{-}$ $B220^{+}$ compartment. n=12; 4 independent experiments. (F) Representative TPLSM images of NALT and submandibular LN. LNs derived from naïve $Aicda^{Cre/+}$ $Rosa26^{Stop\text{-}tdTomato/+}$ mice. Scale bars, 150µm. n=3, 2 independent experiments. (G) Representative plots and quantification of GC B cells of NALT and submandibular LN. LNs derived from naïve C57BL/6 SPF mice. $B220^{+}$ population gated from the $CD45^{+}$ compartment; FAS^{+} $CD38^{-}$ GC population gated from the $B220^{+}$ compartment. n=6, 2 independent experiments. (H) Representative plots and quantification of GC B cell isotypes. NALT and submandibular LN derived from naïve C57BL/6 SPF mice. IgA^{+}, $IgG1^{+}$, $IgG2ab^{+}$ and IgM^{+} population gated from the FAS^{+} $CD38^{-}$ $B220^{+}$ compartment. n=6; 2 independent experiments. (I) Comparison of GC B cell population between naïve SPF and GF mice. FAS^{+} $CD38^{-}$ GC population gated from the $B220^{+}$ compartment. n=8-10; 2 independent experiments.

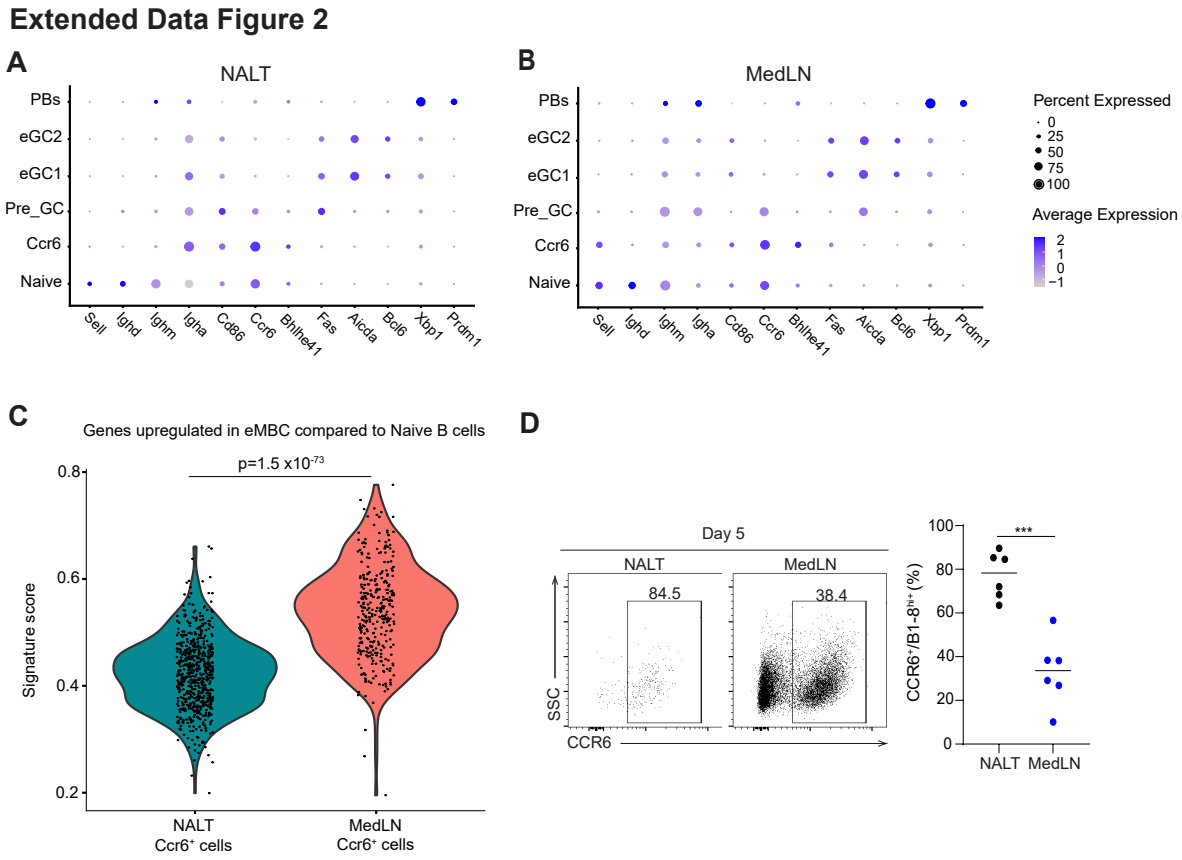

Extended Data Fig. 2: Single-cell RNA sequence analysis of NALT and MedLN-derived antigen-specific B cells.

(A, B) Two-dimensional embedding as in (Fig. 1 I) colored to represent the weight of genes associated with distinct cell clusters. Single-cell RNA-seq of transferred GFP^{+} B1-8^{hi} B cells in the NALT and MedLN, 5 days after i.n. NP-OVA+MPLA. Data was pooled from 5 mice. (C) Violin plots of the distribution of genes upregulated in early memory B cells compared to naïve B cells, in Ccr6^{+} cell cluster, either in the NALT or the MedLN. Data was pooled from 5 mice. (D) Representative flow cytometer plots and quantification of NALT and MedLN at day 5 following i.n. NP-OVA+MPLA. CCR6^{+} population gated from the GFP^{+} B220^{+} CD138^{-} B1-8^{hi} B cells compartment. n=6; 3 independent experiments.

Extended Data Figure 3

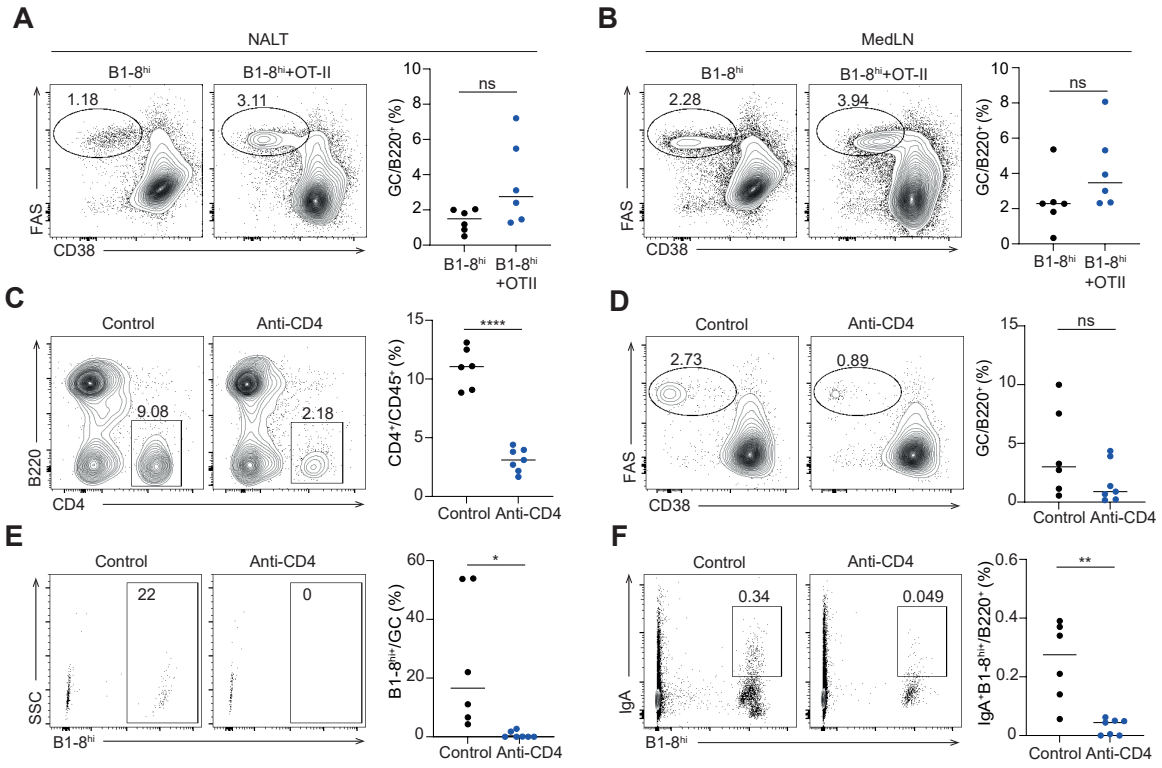

Extended Data Fig. 3: B cell expansion in the SED of the NALT depends on interactions with T cells.

(A, B) Representative plots and quantification of NALT (A) and MedLN (B) at day 7 following i.n. NP-OVA+MPLA with or without injection of $CD4^+$ OT-II T cells. FAS^+ $CD38^-$ GC population gated from the $B220^+$ compartment. n=6; 2 independent experiments. (C-F) Host mice were injected with anti-CD4 antibody while transferring GFP^+ B1-8^{hi} B cells (same procedure as Fig. 2 G). (C) Flow cytometry analysis of $CD4^+$ T cells in NALT at day 7 following NP-OVA intranasal boost. $CD4^+$ T cell population gated from $CD45^+$ compartment. n= 6-7; 2 independent experiments. (D-F) Flow cytometry quantification of B cells in NALT at day 7 following NP-OVA intranasal boost. For D, FAS^+ $CD38^-$ GC population gated from $B220^+$ compartment; for E, GFP^+ B1-8^{hi} population gated from FAS^+ $CD38^-$ GC compartment; for F, IgA^+ GFP^+ B1-8^{hi} B cell population gated from $B220^+$ compartment; n= 6-7; 2 independent experiments.

Extended Data Figure 4

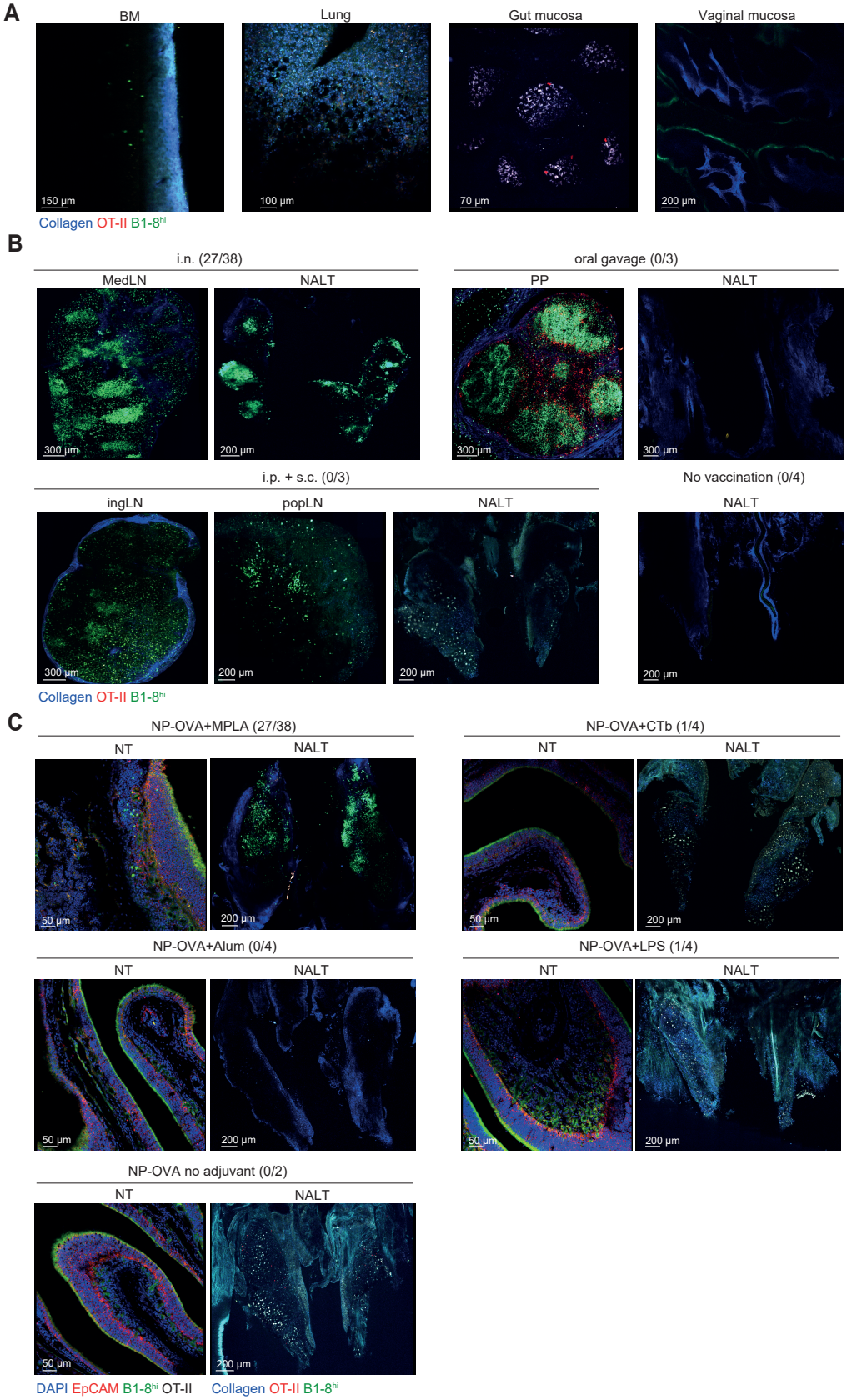

Extended Data Fig. 4: Antigen-specific B cell home to the nasal turbinate from the NALT.

(A) Representative TPLMS images of GFP^+ B1-8^{hi} B cells in different tissues at day 7 post i.n. NP-OVA+MPLA boost. Tissues derived from WT host mice were adoptively transferred with GFP^+ B1-8^{hi} B cells and $Rosa26^{tdTomato/+}$ $CD4^+$ OT-II T cells following i.n. prime and boost immunizations. Scale bars, 70-200μm. (B) Representative TPLMS images of the LNs after different vaccine strategies. i.n.: NP-OVA+MPLA i.n. prime and boost; i.p.+s.c.: NP-OVA+Alum i.p. prime and NP-OVA+MPLA s.c. boost; oral gavage with NP-CT. (C) Representative confocal images of the NT and TPLMS images of the NALTs after vaccination with NP-OVA in different nasal adjuvants. (27/38): 27 mice detected NT-homing GFP^+ B1-8^{hi} B cells out of 38 tested.

Extended Data Figure 5

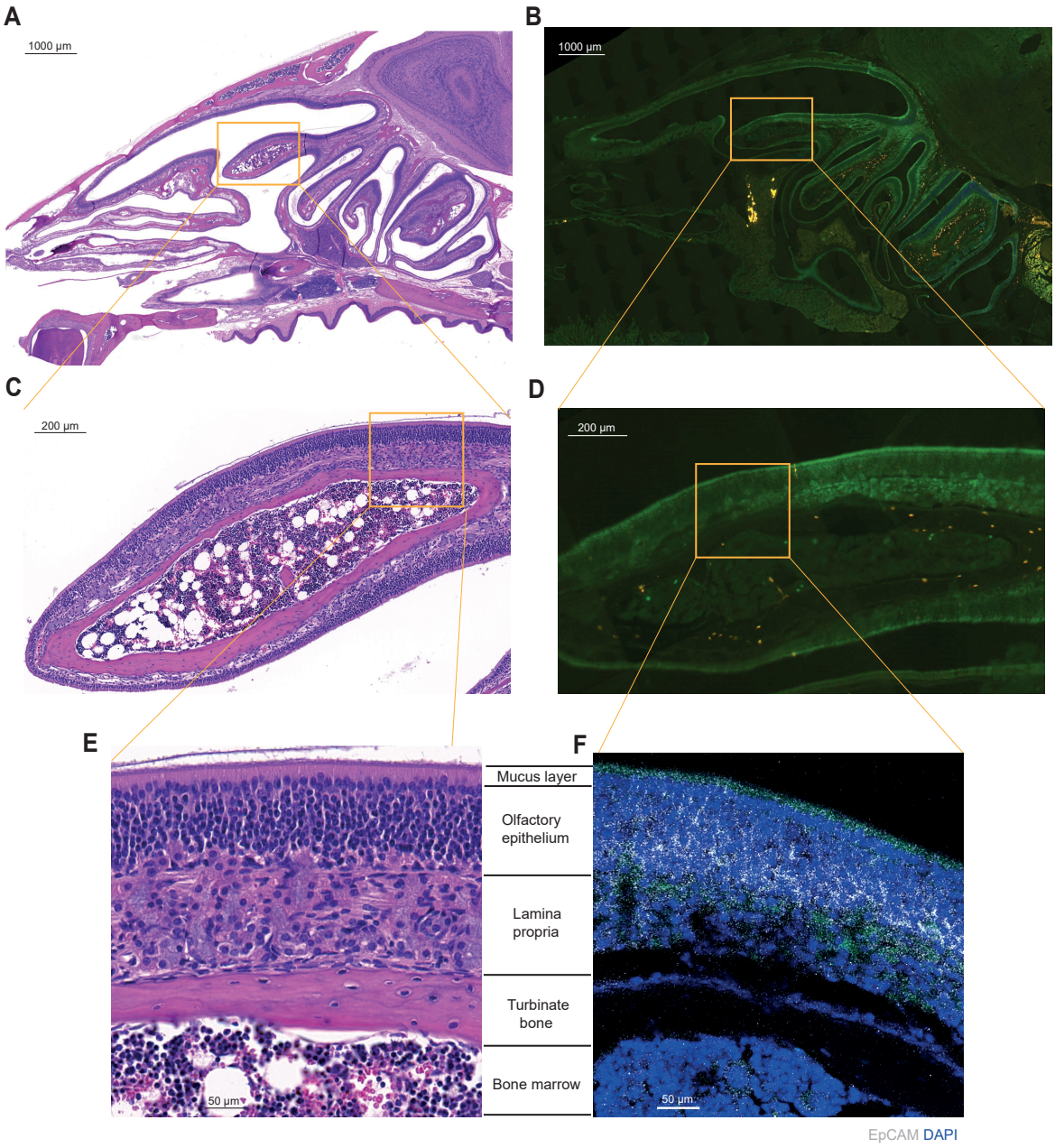

Extended Data Fig. 5. Olfactory epithelium anatomy.

(A, C, E) Anatomy of the NT. Sagittal section of the nasal turbinate of a naïve mouse (8 weeks old) with H&E staining. (B, D, F) Representative digital slide scanner and confocal images of the nasal turbinate of naïve Aicda$^{Cre/+}$ Rosa26$^{Stop\text{-}tdTomato/+}$ Blimp1-YFP^{+} mice. n=4, 2 independent experiments.